Synthesis of a Family of $\{[(VSe_2)_n]_{1.06}(TaSe_2)_m\}_z$ Compounds

Ngoc T. Nguyen,† Brandon Howe,† Juliana R. Hash,† Nicholas Liebrecht,†
Paul Zschack,‡ and David C. Johnson*,†

**Materials Science Institute and Chemistry Department, University of Oregon, Eugene, Oregon 97403, and Advanced Photon Source, Argonne National Laboratory, Argonne, Illinois 60439*

Received October 20, 2006. Revised Manuscript Received January 24, 2007

The first sixteen members of the $\{[(VSe_2)_n]_{1.06}(TaSe_2)_m\}_z$ family of compounds where *n* and *m* were varied from 1 to 4 were synthesized by annealing preconfigured reactants. The factor of 1.06 originates from the *ab*-plane lattice mismatch of VSe_2 and $TaSe_2$, reflecting the non-epitaxial structural relationship between the components. Each individual compound was addressed by sequentially depositing *n* layers of alternating elemental V and Se followed by *m* layers of alternating elemental Ta and Se in which the thickness of each pair of elemental layers was calibrated to yield a single-crystalline layer of the metal diselenide on annealing at low temperature for a short time. The structural changes during the transformation from initial reactant to crystalline superstructure are followed using X-ray diffraction. The structure of these nanoscale superstructures consist of an integral number of VSe_2 and $TaSe_2$ layers with minimal cation mixing between the layers. Electrical measurements show that all of the members of this family are metallic.

Introduction

Recently Cario and co-workers demonstrated the potential of crystal engineering, both predicting and synthesizing new compounds on the basis of two-dimensional building blocks.[1] The concept of using building blocks to predict stable structures leads to families of compounds in which the building blocks are interconnected in different patterns or arrangements.[2] Two-dimensional layers are the simplest building blocks, as the only degrees of freedom in assembling them are the interlayer spacing and the thickness of each building block in the unit cell of the new compound. By assembling two-dimensional building blocks in an AB pattern with different thicknesses of each building block, we can, in principle, design an infinite number of new compounds-$(A)_n(B)_m$ that will at least be kinetically stable. For example, if the two-dimensional building blocks are XMX transition metal dichalcogenide layers, where M is a group IVA, VA, or VIA transition metal and X is a chalcogenide such as S, Se, or Te, an infinite family of $(MX_2)_n(M'X_2)_m$, where M′ is a different group IVA, VA, or VIA transition metal, should in principle exist. These families of nanostructured compounds provide an opportunity to investigate how properties change when the thickness of one or both of the individual components is varied through fundamental length scales associated with physical phenomenon, as properties that depend on this fundamental length will vary as *n* and *m* are changed through this thickness.

A significant challenge in preparing $(A)_n(B)_m$ families of compounds is the very small free-energy differences between members of the family. Traditional bulk synthesis techniques cannot access these compounds, typically yielding a solid solution of the components due to the significant entropy component of the free energy at standard reaction temperatures.[3,4] In only a few systems, such as the misfit layer compounds, has it proven possible to prepare at most one or two members of a family.[5,6] An additional challenge for traditional synthesis techniques comes from the many family members with identical compositions (for example, $(A)_n(B)_n$). Epitaxial growth techniques have been used to overcome these limitations using a variety of deposition techniques (atomic laser deposition, pulsed laser deposition, sputtering, chemical vapor deposition, molecular beam epitaxy) to sequentially deposit the constituents, but this approach typically requires a lattice match between the constituent compounds.[7−16] Even with epitaxial growth techniques, it is

* Corresponding author. Tel: 541-346-4152. Fax: 541-346-0487. E-mail: Davej@uoregon.edu.
† University of Oregon.
‡ Argonne National Laboratory.

(1) Cario, L.; Kabbour, H.; Meerschaut, A. *Chem. Mater.* **2005**, *17*, 234.
(2) Yaghi, O. M.; O'Keefe, M.; Ockwig, N. W.; Chae, H. K.; Eddaoudi, M.; Kim, J. *Nature* **2003**, *423*, 705.
(3) Kalikhman, V. L.; Lobova, T. A.; Pravoverova, L. L. *Neorg. Mater.* **1973**, *9* (6), 923.
(4) Hayashi, K.; Ikeuchi, T.; Takeuchi, H.; Shimakawa, M. *J. Alloys Compd.* **1995**, *219*, 161.
(5) Meerschaut, A. *Curr. Opin. Solid State Mater. Sci.* **1996**, *1* (2), 250.
(6) Wiegers, G. A.; Meerschaut, A. *Mater. Sci. Forum.* **1992**, *101, 102*, 101.
(7) Leskela, M.; Ritala, M. *Thin Solid Films* **2002**, *409*, 138.
(8) Mercey, B.; Salvador, P. A.; Prellier, W.; Doan, T. D.; Wolfman, J.; Hamet, J. F., Hervieu, M.; Raveau, B. *J. Mater. Chem.* **1999**, *9*, 233.
(9) Venkatasubramanian, R.; Colpitts, T.; O'Quinn, B.; Liu, S.; El-Masry, N.; Lamvik, M. *Appl. Phys. Lett.* **1999**, *75*, 1104.
(10) Guldner, Y. *Phys. Scr.* **1982**, *T1*, 32.
(11) Wen, Y.; Song, Y.; Jiang, G.; Zhao, D.; Ding, K.; Yuan, W.; Lin, X.; Gao, H.; Jiang, L.; Zhu, D. *Adv. Mater.* **2004**, *16*, 2018.
(12) Jiang, C.; Markutsya, S.; Tsukruk, V. V. *Adv. Mater.* **2004**, *16*, 157.
(13) Velikov, K. P.; Christova, C. G.; Dullens, R. P. A.; Blaaderen, A. V. *Science* **2002**, *296*, 106.
(14) Wu, X. D.; Xi, X. X.; Li, Q.; Inam, A.; Dutta, B.; DiDomenico, L.; Weiss, C.; Martinez, J. A.; Wilkens, B. J.; Schwarz, S. A.; Barner, J. B.; Chang, C. C.; Nazar, L.; Venkatesan, T. *Appl. Phys. Lett.* **1990**, *56*, 400.

10.1021/cm062509k CCC: $37.00
Published on Web 03/15/2007

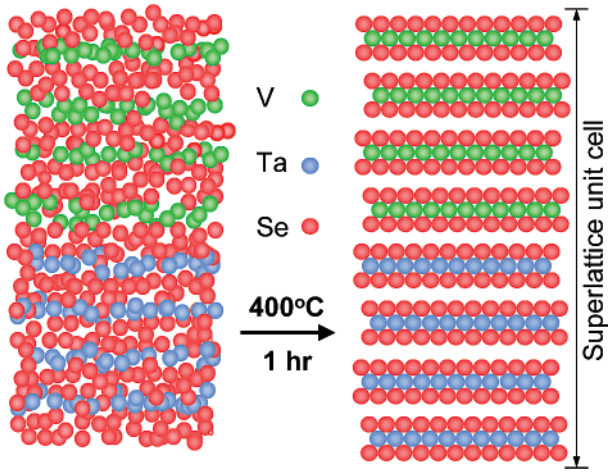

Figure 1. Schematic of one repeating unit of a nanostructured reactant consisting of subnanometer elemental layers that were sequentially deposited. After a brief annealing at 400 °C, the structure self-organizes into well-crystallized dichalcogenide layers.

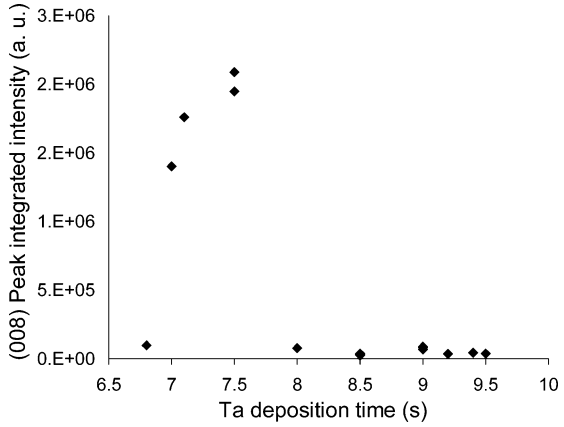

Figure 2. The observed *008* peak intensity after annealing at 400 °C vs Ta deposition time (seconds) for a series of $\{[(VSe_2)_4]_{1.06}(TaSe_2)_4\}_{10}$ superlattices. The deposition conditions for V and Se were also adjusted accordingly to maintain a metal to selenium atomic ratio of 1/2. The deposition time corresponding to the maximum intensity of the *008* diffraction maxima yielded the superlattice with the most and sharpest *00l* diffraction maxima.

frequently difficult to find growth conditions that enable the preparation of both components because of conflicting demands on growth conditions resulting from the high vapor pressure of some elements (such as chalcogenides) and the need for high surface temperatures to obtain sufficient surface mobilities of other elements (such as third-row transition metals). The lack of suitable growth conditions, suitable latticed matched substrates, or lattice match between the components precludes the growth of many potential materials.[17,18] One exception to the lattice match requirement is the van der Waals epitaxy approach pioneered by Koma for compounds containing van der Waals gaps in their structures, such as the dichalcogenides, but such intergrowths are often limited by the conflicting demands on growth conditions stated above.[19−22]

In this paper, we show that it is possible to prepare the first 16 members of the $\{[(VSe_2)_n]_{1.06}(TaSe_2)_m\}_z$ ($m, n = 1-4$) family using modulated elemental reactants, a technique that involves sequentially depositing elements in the appropriate atomic ratios and absolute thicknesses on an ambient temperature substrate followed by a low-temperature anneal. The concept is to design an initial structure that has a composition profile close to that of the desired family member so that only a small amount of thermal energy is needed for the short-range interdiffusion to crystallize the constituents, as shown schematically in Figure 1.[23] Because this approach relies only on controlling composition and diffusion distances and does not require an epitaxial relationship between the components, it potentially provides general access to previously inaccessible families of compounds. We focused on the group V dichalcogenides because they have been extensively investigated because of the discovery of charge density waves (CDW) and the interplay between the CDW and superconductivity.[24,25] Although the effect of different polytypes and varying stoichiometry and composition within solid solutions on properties have been extensively investigated,[26−28] this is the first report of the synthesis of a family of new compounds that consist of ordered intergrowths of group V transition metal dichalcogenide compounds. Electrical transport properties of these compounds revealed potential charge density wave transitions in these nanostructured materials.

Experimental Section

V and Ta metals (99.95% purity) were obtained from Pure Tech and evaporated without further purification. Se shot (99.995% purity) was obtained from Alfa Aesar. The reactants were sequentially deposited in an ultrahigh vacuum chamber (background pressure $< 5 \times 10^{-7}$ Torr) onto unheated prepolished Si wafers (roughness ±3 Å with a native oxide layer on the surface). V was deposited at 0.4 Å/s and Ta at 0.2 Å/s using 3 kW electron beam guns, whereas Se was delivered using a Knudsen effusion cell depositing at 0.5 Å/s. Inficon Xtal microbalance quartz crystal monitors continuously monitored and controlled the deposition rates. A computer program controlled the thicknesses of the elements deposited, opening a shutter either for specified period of time or until a desired change in thickness was reported by the integrated thickness signal of the controlling quartz crystal monitor.

A series of calibration samples were deposited to first determine the ratio of the thicknesses of the elemental layer required to obtain the desired 1:2 metal:chalcogen atomic ratio necessary to form both $TaSe_2$ and VSe_2. Using this information, a second set of calibration

(15) Nakagawara, O.; Shimuta, T.; Makino, T.; Arai, S.; Tabata, H.; Kawai, T. *Appl. Phys. Lett.* **2000**, *77*, 3257.
(16) Iwazaki, Y.; Suzuli, T.; Sekiguchi, S.; Fujimoto, M. *Jpn. J. Appl. Phys.* **1999**, *38*, L1443.
(17) Norman, A. G.; Seong, T.-Y.; Ferguson, I. T.; Booker, G. R.; Joyce, B. A. *Semicond. Sci. Technol.* **1993**, *8*, S9.
(18) Takahasi, M.; Mizuki, J. *J. Cryst. Growth* **2005**, *275*, e2201.
(19) Koma, A. *Thin Solid Films* **1992**, *216*, 72.
(20) Ohuchi, F. S.; Parkinson, B. A.; Ueno, K.; Koma, A. *J. Appl. Phys.* **1990**, *68* (5), 2168.
(21) Shimada, T.; Furukawa, Y.; Furukawa, Y.; Arakawa, E.; Takeshita, K.; Matsushita, T.; Yamamoto, H.; Koma, A. *Solid State Commun.* **1994**, *89* (7), 583.
(22) Shimada, T.; Nishikawa, H.; Koma, A.; Furukawa, Y.; Arakawa, E.; Takeshita, K.; Matsushita, T. *Surf. Sci.* **1996**, *369*, 379.
(23) Noh, M.; Thiel, J.; Johnson, D. C. *Science* **1995**, *270*, 1181.
(24) Wilson, J. A.; DiSalvo, F. J.; Mahajan, S. *Adv. Phys.* **1975**, *24* (2), 117.
(25) Wilson, J. A.; DiSalvo, F. J.; Mahajan, S. *Phys. Rev. Lett.* **1974**, *32* (16), 882.
(26) Yamamoto, M.; Takashi, S. *J. Phys. Soc. Jpn.* **1976**, *41* (4), 1146.
(27) Vaterlaus, H. P. *Helv. Phys. Acta* **1984**, *57* (3), 336.
(28) Yousefi, G. H.; *Mater. Lett.* **1989**, *9* (1), 38.

Table 1. List of the *c*-lattice Parameters (in Ångstrom) Obtained for the 57 Superlattice Compounds Prepared as Part of This Study, Grouped According to the Number of Vanadium Diselenide and Tantalum Diselenide Layers Targeted in the Initial Modulated Elemental Reactant (uncertainties in the last place of each lattice parameter are shown in parentheses)

	no. of $TaSe_2$ layers			
no. of VSe_2 layers	1	2	3	4
1	12.38(1)	18.86(1)	25.60(2)	32.17(3)
	12.41(1)	18.83(1)	25.48(2)	31.98(2)
	12.41(1)			31.96(1)
2	18.49(1)	25.05(4)	31.76(2)	37.92(3)
	18.42(2)	25.32(2)	31.41(3)	37.96(3)
		25.10(2)	31.75(4)	38.29(3)
		24.97(5)		37.87(3)
3	24.73(2)	31.38(3)	37.78(7)	44.35(3)
	24.42(3)	30.98(4)	37.59(5)	44.33(8)
	24.71(9)	31.28(7)	37.48(5)	44.13(5)
			37.65(6)	
4	30.34(1)	36.88(3)	44.05(2)	50.37(3) 50.31(6) 50.28(5) 50.37(4)
	30.67(7)	37.15(2)	43.50(5)	50.24(5) 50.48(6) 50.13(8) 49.96(7)
			43.64(5)	49.66(5) 50.22(7) 49.91(5) 50.38(8)
				50.13(6) 49.5(1)

samples now interleaves varying numbers of alternating Ta and Se layers between a fixed number of V and Se bilayers. The variation in the repeat thicknesses of the as-deposited multilayers as a function of the number of Ta/Se layers deposited yields the thickness of the Ta/Se bilayer from the slope and the thickness of the V/Se bilayer from the intercept. This is repeated, varying the thicknesses to optimize the absolute amount of each of the components deposited until conditions were found in which each deposition sequence of metal and chalcogen yielded one Se−M−Se layer after annealing as determined by the growth of a superlattice diffraction pattern on annealing. The 2.3% difference in the *a*-lattice parameters of $TaSe_2$ and VSe_2 results in an ∼6% increase in the atomic density of the *ab*-planes of VSe_2 relative to $TaSe_2$. This was reflected in our optimized growth conditions and confirmed by X-ray structural analysis, discussed later in this manuscript. The deposition conditions were further optimized by preparing a series of samples designed to yield {[(VSe_2)$_4$]$_{1.06}$($TaSe_2$)$_4$}$_{10}$ superlattices in which the Ta deposition time was varied while V and Se deposition conditions were adjusted to maintain a 1:2 metal:selenium atomic ratio. As shown in Figure 2, the integrated intensity of the superlattice diffraction pattern varied significantly as a function of Ta deposition time. For Ta deposition times between 7.2 and 7.5 s, a maximum in the intensity of the Bragg diffraction pattern was observed, suggesting optimal deposition parameters to form the desired superlattice. To make a {[(VSe_2)$_n$]$_{1.06}$($TaSe_2$)$_m$}$_z$ superlattice, *n* sequences of V and Se were deposited followed by *m* sequences of Ta and Se. This process was repeated *z* times. The typical total thickness was on the order of 50 nm. Samples were annealed in a N_2 atmosphere with less than 0.5 ppm O_2.

Composition was measured using Cameca SX-50 electron microprobe analyzer (20 nA current and 1 μm spot size). Each sample was measured at 10 points across a 1 mm distance. Data were collected at 8, 12, and 16 kV beam energies and analyzed using the Stratagem software suite for thin film samples.[29−32] The Stratagem software uses the variation of the *k* ratios with beam energy to extract the composition of thin films from the convolution of the substrate and film signals. X-ray diffraction measurements were performed on Bruker D8 Discover Diffractometer equipped with Gobel mirror, Bragg−Brentano optics, and a Cu Kα X-ray source ($\lambda_{\alpha1}$ = 1.5405 Å, $\lambda_{\alpha2}$ = 1.5416 Å) operated at 40 kV and 40 mA. Synchrotron diffraction data were also collected using beam line 33 BM-C at the Advance Photon Source at Argonne National Laboratory. The sample was mounted on 4-circle Huber goniometer and $\theta-2\theta$ diffraction patterns were collected using beam line energies at (9.879k eV) and below (9.679 keV) the Ta L_3 absorption edge. The diffraction data collected at different energies were refined using the General Structure Analysis System (GSAS) program. In-plane diffraction was also performed to see *ab*-plane order of the superlattices. In this scan, the sample surface was placed almost parallel to the diffraction plane with an incoming X-ray beam angle of 0.1° off the sample surface. During the measurement, the sample was spun at 60 rpm to reduce or eliminate any texture effects on the measured diffraction. Electrical conductivity measurements were performed from 10 to 300 K using a 4-point van der Pauw technique on a cross pattern defined using a shadow mask.

Results and Discussion

A total of 57 samples were prepared and annealed to form multiple samples of the 16 targeted compounds {[(VSe_2)$_n$]$_{1.06}$-($TaSe_2$)$_m$}$_z$ with $n, m = 1-4$ (the factor of 1.06 in the formula is a consequence of the *a*-lattice parameter mismatch between the component dicalcogenides). The *c*-lattice parameters obtained from these compounds are summarized in Table 1. The systematic changes in the *c* lattice parameter can be used to begin to unravel the structural changes as *n* and *m* vary within this set of {[(VSe_2)$_n$]$_{1.06}$($TaSe_2$)$_m$}$_z$ compounds. Figure 3 graphs these changes to obtain the average change in the lattice parameter as *n* and *m* are systematically increased. The slopes and intercepts of these lines agree well with the literature values of the lattice parameter published for the binary compounds. The $TaSe_2$ layer thickness varies between 6.50 and 6.56 Å from the fits in Figure 3a, with an average value of 6.53 Å. This thickness agrees well with the values for individual Se−Ta−Se layers reported for the 2H-$TaSe_2$.[33,34] The VSe_2 layer thickness obtained from the lines in Figure 3b varies between 6.04 and 6.06 Å, which is consistent with the variation observed in the literature depending both on the polymorph and amount of excess V,

(29) Pouchou, J. L.; Pichoir, F. *Scanning* **1990**, *12*, 212.
(30) Pouchou, J. L.; Pichoir, F.; Boivin, D. In *Proceedings of the 12th International Conference on Experimental Mechanics*, Seattle, Aug 12−18, 1990; Society for Experimental Mechanics: Bethel, CT, 1990.
(31) Pouchou, J. L.; Pichoir, F.; Boivin, D. *Microbeam Analysis*; San Francisco Press: San Francisco, 1990; p 120.
(32) Pouchou, J. L.; Pichoir, F.; Boivin, D. *ONERA Report TP 1990-109*; Office National d'Études et de Recherches Aérospatiales: Châtillon, France, 1990.
(33) *Powder Diffraction File*; International Center for Diffraction Data: Newtown Square, PA, 1999.
(34) Bjerkelund, E.; Kjecshus, A. *Acta Chem. Scand.* **1967**, *21* (2), 513.

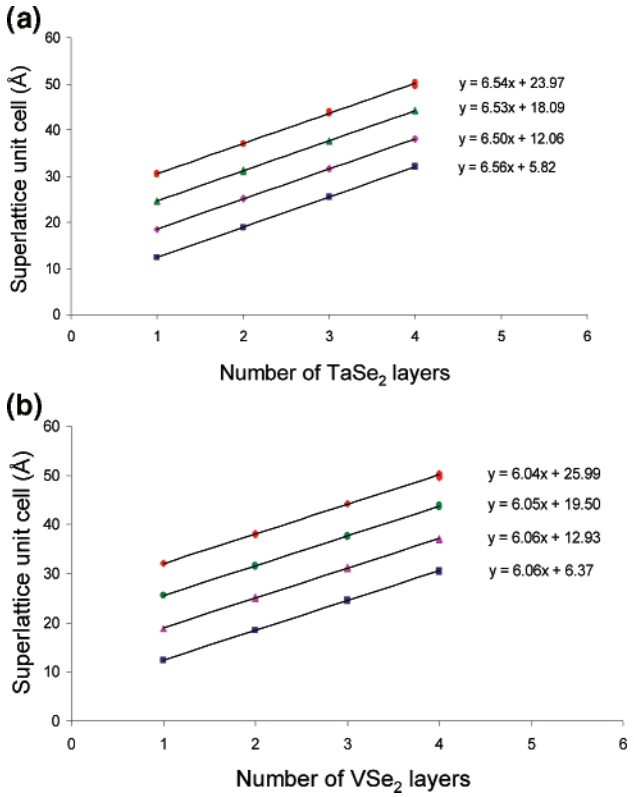

Figure 3. Lattice parameters of the $\{[(VSe_2)_n]_{1.06}(TaSe_2)_m\}_z$ compounds prepared in this study plotted as a function of the number of layers of tantalum diselenide ($m = 1-4$; Figure 3a) or the number of layers of vanadium diselenide ($n = 1-4$; Figure 3b). Lines were fitted through families of compounds in which the number of vanadium diselenide layers is held constant (Figure 3a) or the number of tantalum diselenide layers is held constant (Figure 3b).

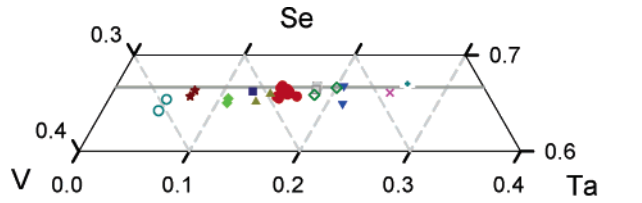

(○, $[(VSe_2)_4]_{1.06}(TaSe_2)_1$; *, $[(VSe_2)_3]_{1.06}(TaSe_2)_1$; ♦, $(VSe_2)_{2n}]_{1.06}(TaSe_2)_n$; ■, $[(VSe_2)_3]_{1.06}(TaSe_2)_2$; ▲, $[(VSe_2)_4]_{1.06}(TaSe_2)_3$; ●, $[(VSe_2)_n]_{1.06}(TaSe_2)_n$; ■, $[(VSe_2)_2]_{1.06}(TaSe_2)_3$; ◊, $[(VSe_2)_3]_{1.06}(TaSe_2)_4$; ▼, $[(VSe_2)_n]_{1.06}(TaSe_2)_{2n}$; ×, $[(VSe_2)_1]_{1.06}(TaSe_2)_3$; +, $[(VSe_2)_1]_{1.06}(TaSe_2)_4$)

Figure 4. The compositions of the superlattices prepared as part of this investigation are shown on this segment of the ternary phase diagram. The line at 66.7 at % Se represents the composition of the ideal $\{[(VSe_2)_n]_{1.06}(TaSe_2)_m\}_z$ superlattices. The samples prepared were generally metal-rich compared to the ideal compositions.

x in $V_{1+x}Se_2$.[33] These systematic changes support the values of n and m assigned to each prepared compound.

Figure 4 shows the composition of the deposited reactants compared to the ideal compositions for the 16 compounds prepared. All of the reactants were slightly metal-rich and tended to be V-rich relative to the ideal composition. This is consistent with the literature, where $V_{1+x}Se_2$ is reported to have been prepared unless the samples are annealed with an overpressure of Se.[33] Films prepared with a slight excesses of Se resulted in diffraction patterns with lower intensity maxima and fewer observable diffraction orders. Within a range of composition, diffraction patterns of similar quality for each compound could be obtained for which the variation

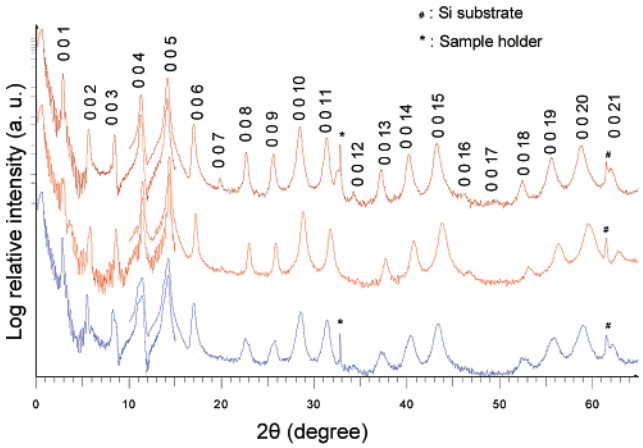

Figure 5. Diffraction patterns (Cu Kα X-ray radiation) obtained for four different preparations of the $\{[(VSe_2)_3]_{1.06}(TaSe_2)_2\}_{14}$ superlattice. The different intensities in the low- and high-angle scans result from the different slits used in the different angle ranges. The relative intensities of the Bragg diffraction peaks are all very similar in all of the scans, implying that the structures of these compounds are all very similar.

in the lattice parameters was found to be 0.6% or less, as illustrated in Figure 5 for $\{[(VSe_2)_3]_{1.06}(TaSe_2)_2\}_{14}$. Although there is a variation in the lattice parameter of 0.4 Å, the relative intensities of the Bragg diffraction maxima are consistent among the different preparations, indicating that the fundamental atomic structure is the same.

The literature provides several potential reasons for the observed variation of the lattice parameters. Bayard and Sienko reported a variation in the c-lattice parameters of $V_{1+x}Se_2$ from 5.9659 to 6.104 Å as x varied from 0.005 to 0.13.[35] The lattice parameter is reported to vary as much as 0.063 Å as a function of stoichiometry for the 2H-$TaSe_2$. Because we have 3 $V_{1+x}Se_2$ layers and 2 $TaSe_2$ layers in the unit cell, the observed lattice parameter variation is not unexpected. The lattice parameters of both of the constituent compounds are also observed to vary by as much as 0.13 Å per dichalcogenide layer between polytypes, a 2% change. As discussed later, the lack of long-range order between different *ab*-planes prevents us from assigning a polytype of the reported compounds. To further probe the extent of the variability of the lattice parameter with respect to small changes in composition, fourteen samples of the $\{[(VSe_2)_4]_{1.06}(TaSe_2)_4\}_{10}$ compound were prepared by slightly varying the amount of deposited materials to explore the composition range in which this compound forms. The lattice parameters ranged from 49.5 ± 0.1 Å to 50.48 ± 0.06 Å for those samples that formed well-ordered superlattices, confirming that there is a width in composition at which members of this family of compounds can be prepared (refer back to Figure 4). Although the absolute magnitude of this lattice parameter change is large, it represents a 2% variation in the lattice parameter. A similar magnitude of lattice parameter change is observed between different polymorphs of the binary compounds, which can be varied with small changes in composition and annealing temperature. Finally, the extent of interdiffusion of the components also changes the lattice parameter and may be responsible for some of the variation,

(35) Bayard, M.; Sienko, J. M. *J. Solid State Chem.* **1976**, *19* (4), 325.

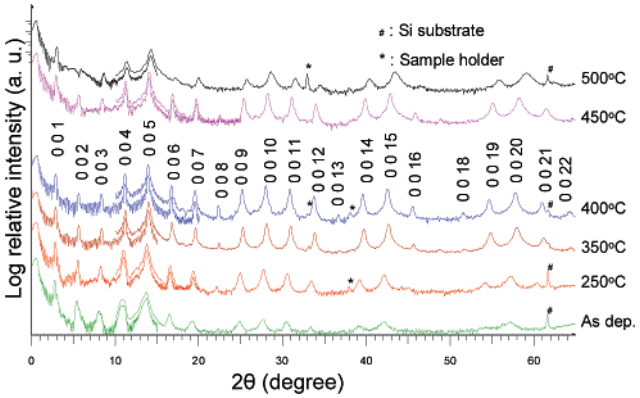

Figure 6. Evolution of the diffraction pattern of the reactant designed to form the compound {[(VSe_2)$_2$]$_{1.06}$($TaSe_2$)$_3$}$_{14}$ as a function of annealing temperature using Cu Kα X-ray radiation. The number and intensity of the *00l* diffraction maxima increase with annealing up to 400 °C and then decrease, indicating that 400 °C is the optimal annealing temperature.

because the extent of interdiffusion is a function of annealing time and temperature as discussed below.

To probe the change in lattice parameter as a function of the extent of interdiffusion, to better understand the formation mechanism of these compounds, and to determine optimal annealing conditions, we collected diffraction data as a function of annealing temperature and time. Figure 6 shows the evolution of the diffraction pattern as a function of annealing temperature for {[(VSe_2)$_2$]$_{1.06}$($TaSe_2$)$_3$}$_{14}$. The low-angle diffraction pattern contains the expected Bragg diffraction peaks resulting from the as-deposited reactants (bottom scan). The high intensity of the *005* diffraction peak results from the thickness of the binary M−Se layers deposited to create the initial reactant. The presence of Bragg diffraction maxima at higher diffraction angles suggests that some long-range order exists in the as-deposited precursor. All of the high-angle diffraction maxima can be indexed as higher-order *00l* Bragg diffraction peaks from the modulated reactant structure. On annealing, we observe the appearance and growth of multiple high order diffraction maxima that can all be indexed as *00l* scattering from the intended {[(VSe_2)$_2$]$_{1.06}$($TaSe_2$)$_3$}$_{14}$ superlattice. The period of the superlattice decreases slightly with annealing temperature, changing from 32.3 ± 0.1 Å in the as deposited reactant to 31.84 ± 0.03 Å at 400 °C and to 31.17 ± 0.08 Å at 500 °C. This decrease in film thickness reflects the increase in packing efficiency of the crystalline layers compared to the relatively disordered structure of the as-deposited sample. The line width of the *005* peak at ∼14° 2θ also decreases significantly as a function of annealing (from 0.32 to 0.039° at 400 °C) as a result of the increase in the size and coherence of the {[(VSe_2)$_2$]$_{1.06}$($TaSe_2$)$_3$}$_{14}$ crystallites. The intensity of the *005* peak increases dramatically, by a factor of 60 by 400 °C, reflecting the increase in ordering of the structure with annealing. The diffraction pattern after annealing a 400 °C contains the most *00l* diffraction maxima from the superlattice structure. Annealing at 500 °C decreases the number of observed diffraction maxima and increases the line width of the *005* peak to 0.351°, suggesting that 400 °C is the most optimal annealing temperature. Annealing studies of several other members of this family of compounds confirmed that annealing at 400 °C for an hour produced

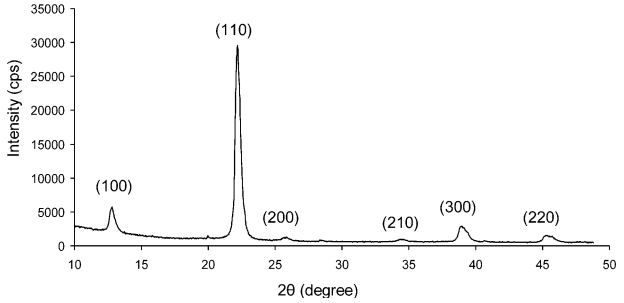

Figure 7. In-plane diffraction pattern of the {[(VSe_2)$_1$]$_{1.06}$($TaSe_2$)$_2$}$_{30}$ superlattice. All expected *hk0* diffraction peaks for metal diselenides were observed. The data were collected using synchrotron radiation at 18 KeV at APS.

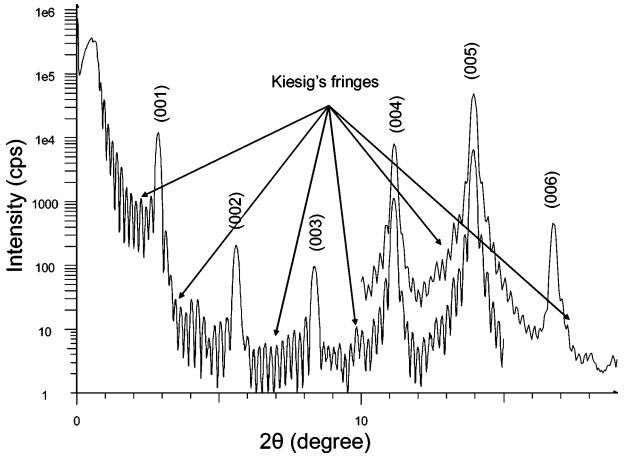

Figure 8. Low-angle X-ray diffraction of the {[(VSe_2)$_2$]$_{1.06}$($TaSe_2$)$_3$}$_{14}$ compound after annealing at 400 °C. The high-frequency oscillation (Kiesig's fringes) was observed out to 17.5° 2θ, which indicated the roughness of the film less than 2.5 Å. Cu Kα X-ray radiation was used and the differences in intensities and resolutions between the two scans result from changes in the slits used in the different scans.

diffraction patterns with the largest number and intensity of diffraction maxima. Annealing above 650 °C results in the destruction of the superlattice structure due to the loss of selenium from the sample. This suggests that additional improvement in the structure can potentially be obtained by annealing the system under controlled Se overpressures.

Also apparent in the annealing data is the dramatic increase in the intensity and angular range of the high-frequency oscillations (Kiesig's fringes) resulting from the interference of X-rays scattered from the front and back surfaces of the film. The low-angle region (0−20° 2θ) of the diffraction pattern of {[(VSe_2)$_2$]$_{1.06}$($TaSe_2$)$_3$}$_{14}$ after annealing at 400º illustrates the extent of this effect, as shown in Figure 8. From the position of these subsidiary maxima, the total film thickness can be calculated. The position of the maxima θ_i of the specularly reflected X-ray beam is given by

$$m_i\lambda = 2d(\sin^2\theta_i - \sin^2\theta_c)^{1/2}$$

where d is the thickness of the film , m_i the order of the i-th maxima, and θ_c the critical angle. Absolute film thickness is determined by rearranging the equation and extracting the thickness d from the slope, as given by the equation below.

$$\sin^2\theta_i = \left(\frac{\lambda}{2}\right)^2\frac{m_i^2}{d^2} + \sin^2\theta_c$$

The calculated total thickness value of 440 ± 5 Å agrees well with the total thickness from the calculated superlattice unit-cell thickness (31.84 Å) and number of superlattice unit cells (14) deposited. The observation of high-frequency oscillations out to 17.5° 2θ implies that the annealed film is very smooth. Using the relationship developed by Parratt,[36] we calculate a decrease in roughness from ~10 Å in the as-deposited state down to less than 2.5 Å after annealing at 400 °C. We believe this dramatic increase in the smoothness of the films results from the rapid two-dimensional growth along the *ab*-planes of the transition-metal dichalcogenides. The film after annealing at 400 °C contains large domains of constant thickness with 14 unit cells of the $\{[(VSe_2)_2]_{1.06}(TaSe_2)_3\}_{14}$ compound aligned with the *c*-axis perpendicular to the substrate, corresponding to the 14 periods deposited in the initial modulated elemental reactant.

The presence of only *00l* diffraction maxima in the diffraction patterns indicates preferred crystallographic alignment of the crystallites. The preferred alignment was quantified by rocking curve diffraction measurements that showed that the *ab*-planes of the superlattice are within 0.03° of being parallel with the surface of the substrate after annealing at 400 °C. To obtain information about the structure in the other crystallographic directions of this highly textured sample, we collected data throughout the reciprocal space. Diffraction data collected at the APS in a grazing geometry to the surface (0.1° off the sample surface) allowed us to observe diffraction from the *ab*-planes. Figure 7 showed the in-plane diffraction pattern of the sample $\{[(VSe_2)_1]_{1.06}(TaSe_2)_2\}_{30}$, which Rietveld refinement indicated had a significant amount (10%) of Ta substituted for V in the nominally VSe_2 layer. All the main peaks can be indexed as an *hk0* family of Bragg peaks, yielding an *a*-lattice parameter of 3.472 ± 0.004 Å. The small peaks near 21, 28, and 41° 2θ were not identified and may come from the Si substrate and/or the sample holder. The *a*-lattice parameter is close to the *a*-lattice parameter of 1T-$TaSe_2$ (3.4769 Å) and significantly larger than that observed for $V_{1.005}Se_2$ (3.356 Å).[33] The observed splitting of the *300* and *220* peaks may result from the difference between the *a*-lattice parameter of the predominately VSe_2 sub-block and the predominately $TaSe_2$ sub-block. The *a*-lattice parameter decreased from 3.472 ± 0.004 Å to 3.436 ± 0.003 Å as the number of $TaSe_2$ layers increase from 2 to 4 in the series $\{[(VSe_2)_1]_{1.06}(TaSe_2)_2\}_{30}$ to $\{[(VSe_2)_1]_{1.06}(TaSe_2)_4\}_{14}$. Because an increase in lattice parameter would be expected because of the increase in the percentage of Ta, this decrease may result from a change in polytype of $TaSe_2$ in the superlattice structure from 1T to 3R or 2H when the number of $TaSe_2$ layers is increased. Determining the polytypes of each sub-block will be very difficult given the small structural coherence along *hkl* directions, as discussed below.

Attempts to find mixed *hkl* reflections result in the observation of weak, very broad reflections at the expected locations for the individual dichalcogenide components without any observed intensities that would be expected for a supercell structure. Given the observed diffraction *hk0* maxima from the *ab*-plane and the *00l* reflections along the *c* direction, this result implies significant disorder between different *ab*-planes. The broad reflections suggest there is some order in at least some of the individual VSe_2 and $TaSe_2$ blocks but that there is no long-range stacking order between blocks. This disorder is frequently observed in layered clay minerals[37] and reflects the relatively small energy differences between different stacking sequences resulting from the weak van der Waals bonding between the layers.

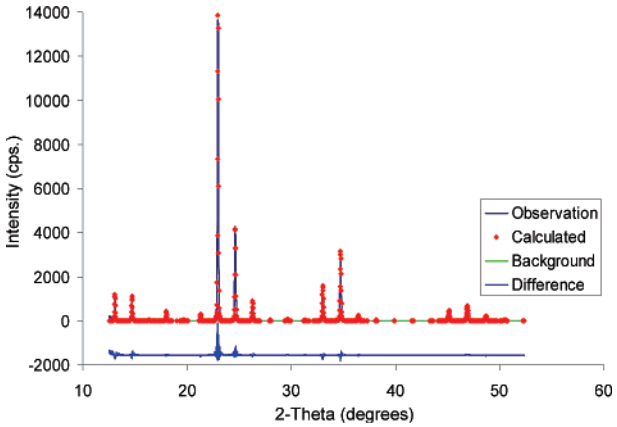

Figure 9. GSAS refinement result of the $\{[(VSe_2)_3]_{1.06}(TaSe_2)_4\}_{10}$ superlattice compound. The data were collected at Advance Photon Source (Argonne National Laboratory) using Tantalum L_3 absorption edge (9.879 KeV energy).

Rietveld refinements using the general structure analysis system (GSAS)[38] program were done on most of the 57 samples prepared as part of this investigation to determine the atomic *z* coordinates of the atom planes that comprise the structure along the *c*-axis (see the Supporting Information). Because only *00l* diffraction data were available, the refinement procedure refined only the *z* coordinate of the atomic positions. The refinement cycle was stopped when the χ^2 value (goodness of fit) was less than 10 and the *R* (residual) values for both fitted diffracted peaks and background were less than 0.1. To confirm the structures obtained, we selected the $\{[(VSe_2)_3]_{1.06}(TaSe_2)_4\}_{10}$ compound for scattering studies at different energies using the beam line 33BM-C at the Advance Photon Source at Argonne National Laboratory. The beam line energies selected were at (9.879 keV) and just below (9.679 keV) the Ta L_3 absorption edge. The data at these energies and at the copper Kα X-ray source radiation were refined simultaneously. Figure 9 showed the result of refinement, comparing the experimental data at the Ta L_3 adsorption edge with calculated intensities based on the refinement model. The total residual values for both fitted peaks and background for both data sets are less than 0.1, whereas the goodness of fit (χ^2) is still high (~40) because of the presentation of the Kiesig's fringes, which were not fitted using GSAS. The graphical representation of the refined structure of the $\{[(VSe_2)_3]_{1.06}(TaSe_2)_4\}_{10}$ compound is shown in Figure 10. The VSe_2 substructure was found to be very similar to that observed in the binary compound, with intralayer and van der Waal gap distances close to those

(36) Wainfan, N.; Parratt, L. G. *J. Appl. Phys.* **1960**, *31* (8), 1331.

(37) Brindley, G. W.; Brown, G. *Crystal Structure of Clay Minerals and their X-ray Identification*; Mineralogical Society: London, 1980.

(38) Larson, C. A.; Von Dreele, B. R. *General Structure Analysis System*; Los Alamos National Laboratory: Los Alamos, NM, 2004.

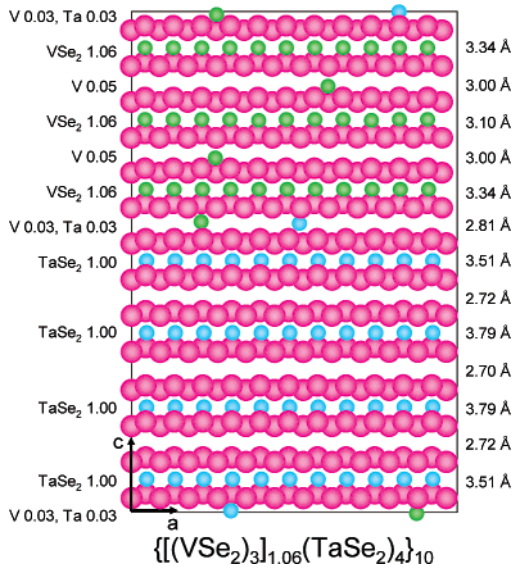

Figure 10. Graphical representations of the refined structure of the {-[(VSe_2)$_3$]$_{1.06}$($TaSe_2$)$_4$}$_{10}$ superlattice compound prepared in this study. The occupancies of the different metal layers are shown on the left and the intra- and interlayer repeat distances are shown on the right.

reported in the literature for the parent compound.[39] Just as V is found to easily self-intercalate VSe_2, resulting in a stoichiometry of $V_{1+x}Se_2$, a small amount (3−5%) of V was found to be intercalated in the VSe_2 van der Waals gap in all of the superlattice compounds investigated in this study. The $TaSe_2$ substructure was found to be very similar to the reported structure for the 2H-$TaSe_2$.[40] Intercalating Ta in the van der Waal gaps of the $TaSe_2$ substructure did not increase the quality of the fit, suggesting that intercalation occurs only in van der Waals gaps adjacent to VSe_2 layers. The van der Waals gaps between the VSe_2 and $TaSe_2$ blocks were found to be slightly larger that those observed in the VSe_2 block and smaller than those of $TaSe_2$ block. A small amount of both Ta and/or V were found to be in the van der Waal gap between the components. There was a trend of the $TaSe_2$ gaps decreasing in size when moving toward the $TaSe_2$−VSe_2 interfaces, whereas the VSe_2 gaps increased in size toward the interfaces. This is perhaps a consequence of the misfit between the substructures in the *ab*-plane. We observed that the atomic densities of the *ab*-plane of the VSe_2 sub-block in the superlattice were found to be 6% higher than the atomic density of the *ab*-plane in the $TaSe_2$ part. This atomic density difference agrees well with that expected from the known structures of the binary compounds (5.29% higher atomic density in VSe_2 calculated from the 2.3% smaller *a*-lattice parameter of VSe_2). For most of the compounds investigated, cation mixing between the VSe_2 and $TaSe_2$ layers is limited to only a few percent, even for the layers at the VSe_2−$TaSe_2$ interfaces. Significant cation mixing of V in $TaSe_2$ was found only in the {[(VSe_2)$_n$]$_{1.06}$-($TaSe_2$)$_1$}$_z$ (n = 1−4) series, in which up to 20% of V was found to be required in the $TaSe_2$ layer to obtain a reasonable refinement. The refinement results confirm the synthesis of the title family of compounds using modulated elemental

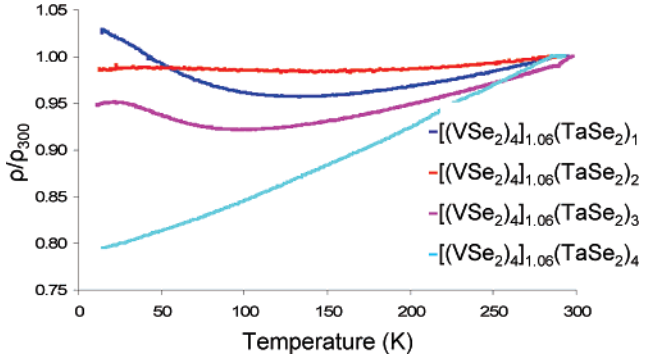

Figure 11. Electrical resistivity data as a function of temperature obtained for {[(VSe_2)$_4$]$_{1.06}$($TaSe_2$)$_n$}$_z$ (n = 1−4) superlattices.

reactants and the intercalated V in the VSe_2 layers required in the refinement accounts for the extra V observed in the elemental compositions measured using electron microprobe analysis.

The component compounds, $TaSe_2$ and VSe_2, are both metals, and both have been the subject of investigations exploring electron localization due to the onset of a charge density wave (CDW).[25] $TaSe_2$ was discovered to have a CDW anomaly in its resistivity between 90 and 122 K.[41,42] VSe_2 was also found to have an anomaly in its resistivity at 80 K that was found to be very sensitive to the extent of V intercalation.[35] Figure 11 shows the electrical resistivity values obtained {[(VSe_2)$_4$]$_{1.06}$($TaSe_2$)$_m$}$_z$ (m = 1−4). The compounds, which are representative of the samples studied, all have metal-like character with their resistivities ranging from 2.47×10^{-4} to 7.78×10^{-4} Ω cm, which is expected from the metallic properties of both components. We observed an upturn in the resistivities with decreasing temperature for both {[(VSe_2)$_4$]$_{1.06}$($TaSe_2$)$_1$}$_{20}$ and {[(VSe_2)$_4$]$_{1.06}$-($TaSe_2$)$_3$}$_{15}$ in the 100−150 K range. This may result from electron localization due to a CDW; however, we did not see any similar behavior from other compounds in the study. This is perhaps as a result of V intercalation in the van der Waal gaps, as suggested by Sienko and Bayard to explain the variation of electrical behavior with stoichiometry for VSe_2.[43] To reduce the amount of intercalation of V and reduce the density of other defects, it will be necessary to anneal these samples under slight overpressures of Se relative to the stoichiometric binary compounds. This may also permit annealing of the samples for longer times and/or higher temperatures with limited interdiffusion to obtain samples with increased ordering between the *ab*-planes.

Conclusion

The successful synthesis of a family of new {[(VSe_2)$_n$]$_{1.06}$-($TaSe_2$)$_m$}$_z$ compounds is presented using a approach that gives kinetic control over both n and m within this family of compounds. The results of structural studies of these compounds show that the building block approach to their design yielded structures with the expected n and m values

(39) Rigoult, J.; Guidi-Morosini, C. *Acta Crystallogr., Sect. B* **1982**, *38*, 1157.
(40) Brown, B. E.; Beerntsen, D. J. *Acta Crystallogr*. **1965**, *18*, 31.
(41) Suits, B. H.; Chen, M. C. *Phys. Lett.* **1980**, *79A* (2, 3), 224.
(42) Harper, J. M. E.; Geballe, T. H.; DiSalvo, F. J. *Phys. Rev. B* **1977**, *15* (6), 2943.
(43) Bayard, M.; Sienko, J. M. *J. Phys., Colloq.* **1976**, *37*, C4−169.

and that the structure of the binary components are very similar to those reported for the bulk binary compounds. All of the compounds prepared were found to be metallic.

Acknowledgment. This study was funded by the National Science Foundation (DMR 0103409). The authors thank Ms. Jenia Karapetrova at the Advance Photon Source for assistance working on the beam line. Use of the Advanced Photon Source was supported by the U.S. Department of Energy, Office of Science, Office of Basic Energy Sciences, under Contract W-31-109-ENG-38.

Supporting Information Available: Rietveld refinements, diffraction patterns, schematic structures with intra- and interplane distances. This material is available free of charge via the Internet at http://pubs.acs.org.

CM062509K